

ECOLOGY

Phenotypic plasticity of carbon fixation stimulates cyanobacterial blooms at elevated CO₂Xing Ji^{1,2*}, Jolanda M. H. Verspagen^{1*}, Dedmer B. Van de Waal³, Björn Rost^{4,5}, Jef Huisman^{1†}

Although phenotypic plasticity is a widespread phenomenon, its implications for species responses to climate change are not well understood. For example, toxic cyanobacteria can form dense surface blooms threatening water quality in many eutrophic lakes, yet a theoretical framework to predict how phenotypic plasticity affects bloom development at elevated $p\text{CO}_2$ is still lacking. We measured phenotypic plasticity of the carbon fixation rates of the common bloom-forming cyanobacterium *Microcystis*. Our results revealed a 1.8- to 5-fold increase in the maximum CO₂ uptake rate of *Microcystis* at elevated $p\text{CO}_2$, which exceeds CO₂ responses reported for other phytoplankton species. The observed plasticity was incorporated into a mathematical model to predict dynamic changes in cyanobacterial abundance. The model was successfully validated by laboratory experiments and predicts that acclimation to high $p\text{CO}_2$ will intensify *Microcystis* blooms in eutrophic lakes. These results indicate that this harmful cyanobacterium is likely to benefit strongly from rising atmospheric $p\text{CO}_2$.

INTRODUCTION

Phenotypic plasticity is one of the major challenges in the study of how organisms will respond to environmental change (1–3). Phenotypic plasticity implies that the traits of organisms are not constant, as the same genotype may display different phenotypes depending on the prevailing environmental conditions. For example, the temperature and CO₂ response of a species may vary depending on the climatic conditions to which individuals of this species have been previously exposed (3, 4). Taking the phenotypic plasticity of traits into account is therefore essential for accurate predictions of how species will respond to climate change.

Cyanobacterial blooms appear to increase in frequency, intensity, and duration in many eutrophic lakes, reservoirs, and estuaries, often in association with increasing nutrient loads, changes in land use, and global warming (5–8). Dense cyanobacterial blooms can have severe environmental impacts, as bloom-forming species are able to produce a variety of potent toxins affecting birds and mammals including humans, and may therefore negatively affect the use of water for recreation, drinking water, and fisheries (8–10). Recent research indicates that surface blooms of cyanobacteria may benefit not only from high temperatures but also directly from the increase in partial pressure of carbon dioxide ($p\text{CO}_2$) in the atmosphere (11–13). The photosynthetic activity of dense cyanobacterial blooms depletes dissolved CO₂ concentrations in the upper water column and increases pH (11, 14), thereby shifting the inorganic carbon equilibrium toward bicarbonate (HCO_3^-) and carbonate (CO_3^{2-}). Rising atmospheric $p\text{CO}_2$ in combination with depletion of the dissolved CO₂ concentration by surface blooms will increase the $p\text{CO}_2$ gradient across the air-water interface. This may result in an enhanced influx of CO₂ into the water column (15) that fuels the photosynthetic carbon fixation of cyanobacterial blooms (11, 13).

Phenotypic plasticity is likely to play an important role in the response of cyanobacterial blooms to rising CO₂. Cyanobacteria use a sophisticated CO₂-concentrating mechanism (CCM) (16, 17). Most inorganic carbon taken up by the cells is first converted to bicarbonate and then transported to cellular compartments called carboxysomes, where bicarbonate is converted back to CO₂ and fixed into organic carbon by the RuBisCO enzyme. The cyanobacterial CCM comprises up to five different carbon uptake systems, including two CO₂ uptake systems (NDH-1₃ and NDH-1₄) and three bicarbonate uptake systems (BCT1, BicA, and SbtA) (18). These uptake systems differ in kinetic properties. For example, BicA has a low affinity for bicarbonate but high flux rate, whereas SbtA has a high affinity but low flux rate (18, 19). Moreover, cyanobacteria may combine and regulate these uptake systems in different ways (12, 18–20). Also, the number of carboxysomes per cell may vary in response to changes in CO₂ availability (21). This flexibility of the CCM creates the potential for a high degree of phenotypic plasticity of carbon fixation rates in cyanobacterial blooms.

Thus far, phenotypic plasticity of CO₂ and bicarbonate uptake kinetics have been quantified for only a limited number of cyanobacteria. This includes the freshwater laboratory strains *Synechocystis* PCC 6803 (22) and *Synechococcus* PCC 7942 (23, 24), as well as the marine cyanobacteria *Trichodesmium* IMS101 (25) and *Prochlorococcus* MED4 (26). However, phenotypic plasticity of the carbon uptake kinetics of bloom-forming freshwater cyanobacteria is essentially unknown, and a methodology to incorporate this plasticity into predictive models of cyanobacterial and other harmful algal blooms is still lacking.

Here, we develop a novel theoretical framework to predict how phenotypic plasticity will affect the proliferation of cyanobacteria in response to rising atmospheric $p\text{CO}_2$. For this purpose, we investigate phenotypic plasticity of the carbon uptake kinetics of *Microcystis*, one of the most ubiquitous and notorious bloom-forming cyanobacteria (8, 27). Two toxic *Microcystis* strains were cultured in the laboratory to measure their CO₂ and bicarbonate uptake kinetics after acclimation to low and to high $p\text{CO}_2$ (Fig. 1, A and B). The observed phenotypic plasticity of the kinetic parameters was implemented in a mathematical model to predict cyanobacterial growth and dynamic changes in CO₂ uptake and inorganic carbon chemistry (Fig. 1, C and D). The model predictions were validated using controlled laboratory chemostat experiments exposed to low and to

¹Department of Freshwater and Marine Ecology, Institute for Biodiversity and Ecosystem Dynamics, University of Amsterdam, P.O. Box 94240, 1090 GE Amsterdam, Netherlands. ²Shanghai Key Laboratory for Urban Ecological Processes and Eco-Restoration and Center for Global Change and Ecological Forecasting, School of Ecological and Environmental Science, East China Normal University, Shanghai, PR China. ³Department of Aquatic Ecology, Netherlands Institute of Ecology, Wageningen, Netherlands. ⁴Alfred Wegener Institute, Helmholtz Centre for Polar and Marine Research, Bremerhaven, Germany. ⁵University of Bremen, Bremen, Germany. *These authors contributed equally to this work.

†Corresponding author. Email: j.huisman@uva.nl

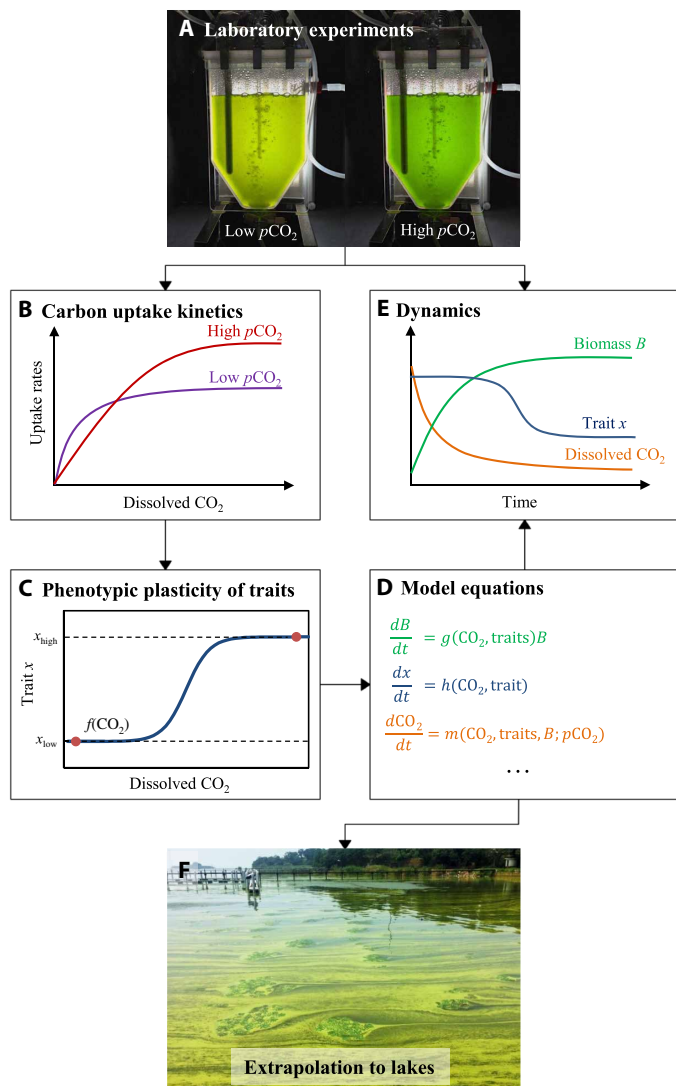


Fig. 1. Conceptual approach of this study. (A) *Microcystis* strains were grown at low and at high $p\text{CO}_2$ in laboratory chemostats. (Photo credit: Xing Ji, University of Amsterdam.) (B) Carbon uptake kinetics of *Microcystis* cells acclimated to low and high $p\text{CO}_2$ were measured, and (C) the plasticity of the measured uptake kinetics was incorporated in a mathematical model. (D) The model was used to predict dynamic changes in population density, uptake kinetics, and inorganic carbon chemistry, and (E) these predictions were validated by the chemostat experiments. (F) The validated model was scaled up to lakes to predict how phenotypic plasticity of *Microcystis* affects its bloom development in response to rising atmospheric $p\text{CO}_2$. This photo shows a large *Microcystis* bloom in Lake Taihu, China. (Photo credit: Xing Ji, University of Amsterdam.)

high $p\text{CO}_2$ (Fig. 1E). Subsequently, the validated model was scaled up from the laboratory to eutrophic lakes to predict how physiological acclimation of the carbon fixation rates will affect the response of *Microcystis* blooms to rising atmospheric $p\text{CO}_2$ (Fig. 1F).

RESULTS

Phenotypic plasticity of carbon uptake kinetics

Microcystis strains PCC 7806 and PCC 7941 were grown in laboratory chemostats provided with nutrient-rich medium and aerated with either low $p\text{CO}_2$ [100 parts per million (ppm)] or high $p\text{CO}_2$ (1000 ppm).

These $p\text{CO}_2$ settings reflect the wide variation in dissolved CO_2 concentrations in lakes, ranging from CO_2 -undersaturated to CO_2 -supersaturated waters (11, 28). After the chemostats were in steady state for ~ 20 days, we took samples to measure CO_2 and bicarbonate uptake kinetics of the *Microcystis* cells with a membrane inlet mass spectrometer (MIMS) using a chemical disequilibrium assay (29, 30). With a dilution rate of 0.2 day^{-1} , the experiments allowed for ~ 6 generations of physiological acclimation to the imposed CO_2 conditions, which is comparable to the time scale of cyanobacterial bloom development. The results show that the carbon uptake kinetics of *Microcystis* cells acclimated to high $p\text{CO}_2$ were very different from the uptake kinetics of cells acclimated to low $p\text{CO}_2$ (Fig. 2 and fig. S1 for *Microcystis* PCC 7806 and PCC 7941, respectively).

To quantify the uptake kinetics, the measured CO_2 and bicarbonate uptake rates (V) were fitted to the Michaelis-Menten equation

$$V = \frac{V_{\max} [C]}{K_{1/2} + [C]} \quad (1)$$

where $[C]$ is the CO_2 or bicarbonate concentration, V_{\max} is the maximum uptake rate, and $K_{1/2}$ is the half-saturation constant (i.e., the carbon concentration at which the uptake rate equals half of V_{\max}). The ratio $V_{\max}/K_{1/2}$ represents the initial slope of the uptake kinetics at $[C] = 0$ and provides a measure of the uptake efficiency at low carbon concentration.

For *Microcystis* PCC 7806, the maximum net CO_2 uptake rate ($V_{\max, \text{CO}_2, \text{net}}$) was more than five times higher at high $p\text{CO}_2$ than at low $p\text{CO}_2$, whereas the maximum bicarbonate uptake rate (V_{\max, HCO_3}) was not significantly affected by $p\text{CO}_2$ (Fig. 2; Fig. 3, A and B). Half-saturation constants for CO_2 and bicarbonate uptake were both significantly higher in cells acclimated to high $p\text{CO}_2$ (Fig. 3, C and D). The CO_2 uptake efficiency (i.e., the initial slopes in the insets of Fig. 2, A and B) was not much affected by $p\text{CO}_2$. The bicarbonate uptake efficiency, however, was almost three times lower at high $p\text{CO}_2$ than at low $p\text{CO}_2$ (insets in Fig. 2, C and D).

For *Microcystis* PCC 7941, $V_{\max, \text{CO}_2, \text{net}}$ was 1.8 times higher, whereas V_{\max, HCO_3} was $\sim 40\%$ lower at high than at low $p\text{CO}_2$ (fig. S1 and Fig. 3, A and B). Its half-saturation constants for CO_2 and bicarbonate uptake were not significantly affected by $p\text{CO}_2$ (Fig. 3, C and D).

Hence, after acclimation to high $p\text{CO}_2$, both *Microcystis* strains achieved much higher maximum CO_2 uptake rates, but they became less efficient in bicarbonate uptake through either an increased half-saturation constant or a reduced maximum bicarbonate uptake rate.

Modeling phenotypic plasticity

We incorporated the observed plasticity of the carbon uptake kinetics into a mathematical model. The model considers quantitative plastic traits and assumes that trait values dynamically adjust to the prevailing environmental conditions. If x denotes the value of a plastic trait (such as V_{\max} and $K_{1/2}$), then dynamic changes of this trait value are described as

$$\frac{dx}{dt} = c(f[\text{CO}_2] - x(t)) \quad (2)$$

where the function $f[\text{CO}_2]$ describes the acclimated trait value as a function of the dissolved CO_2 concentration, $x(t)$ is the actual trait value at time t , and c is the acclimation rate. The function $f[\text{CO}_2]$ is replaced by $f[\text{HCO}_3^-]$ for traits involved in bicarbonate uptake.

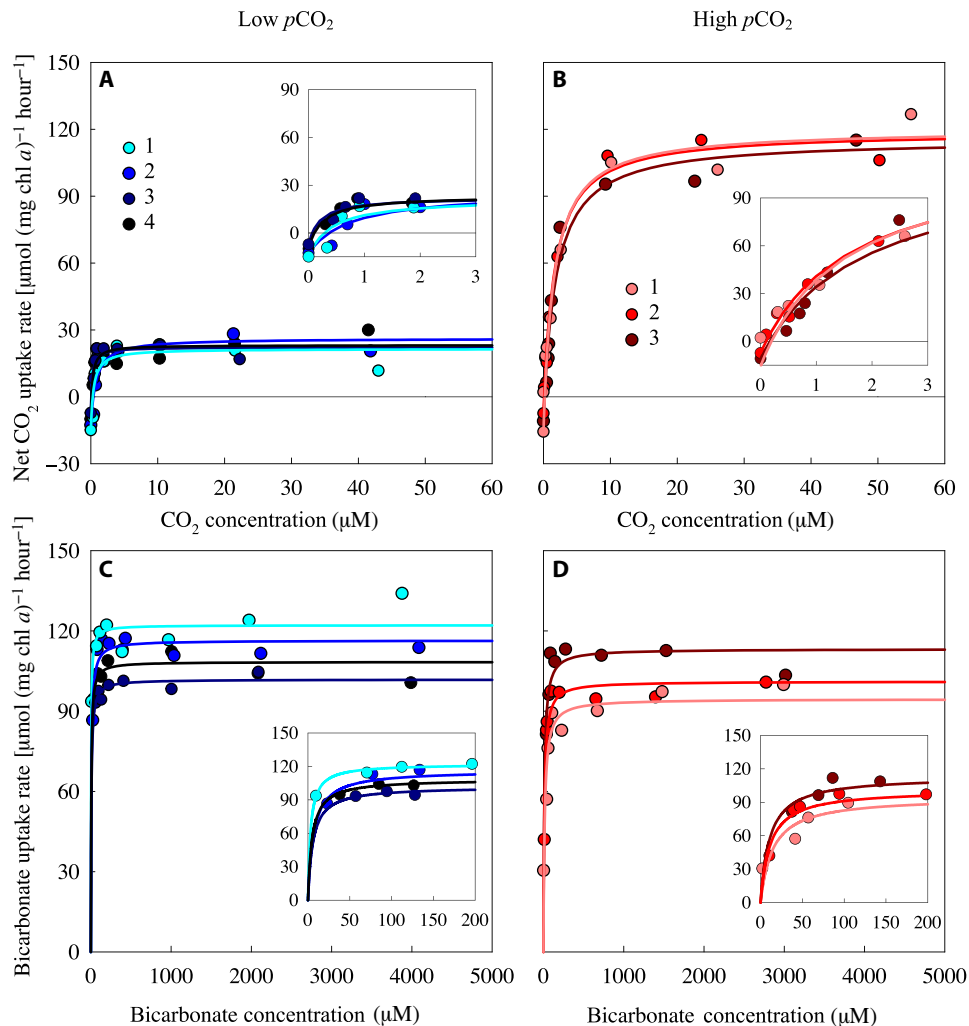


Fig. 2. Carbon uptake kinetics of *Microcystis* PCC 7806 acclimated to either low or high $p\text{CO}_2$. (A and B) Net CO_2 uptake rate as function of the dissolved CO_2 concentration, after acclimation to (A) low $p\text{CO}_2$ and (B) high $p\text{CO}_2$. (C and D) Bicarbonate uptake rate as function of the bicarbonate concentration, after acclimation to (C) low $p\text{CO}_2$ and (D) high $p\text{CO}_2$. Carbon uptake kinetics were measured after ~ 20 days of acclimation to the steady-state conditions in the chemostats. Measurements were replicated fourfold at low $p\text{CO}_2$ and threefold at high $p\text{CO}_2$, as indicated by the different colors. Lines are Michaelis-Menten fits to each of the replicates (see table S2 for parameter estimates). Insets zoom in at the carbon uptake kinetics at low dissolved CO_2 and bicarbonate concentrations.

We assume that the function f has an S-shaped form, such that the acclimated trait value is bound between physiological limits, x_{low} and x_{high} (Fig. 1C; see section S2 for details).

All traits significantly affected by $p\text{CO}_2$ in the experiments are considered to be plastic. For instance, in our application, the plastic traits of *Microcystis* PCC 7806 are its maximum CO_2 uptake rate and half-saturation constants for CO_2 and bicarbonate (Fig. 3). The physiological limits of these traits are set at the trait values observed at low and at high $p\text{CO}_2$.

The resultant description of the phenotypic plasticity of the carbon uptake kinetics was combined with dynamic equations describing population growth and the feedbacks of population growth on inorganic carbon chemistry, light, nutrients, pH, and alkalinity (see section S2 for details).

Validating the model in laboratory experiments

To test the model predictions, we ran duplicate chemostat experiments with *Microcystis* PCC 7806 at both low and high $p\text{CO}_2$ (Fig. 1A).

The *Microcystis* populations increased during the first 2 weeks of the experiments, reducing light availability, modifying inorganic carbon chemistry, and increasing pH, after which the cyanobacterial populations and other experimental variables approached a steady state (Fig. 4). The steady states were maintained for several weeks. *Microcystis* PCC 7806 produced much higher steady-state population densities at high than at low $p\text{CO}_2$ (Fig. 4, A and B, and table S1). In the experiments at low $p\text{CO}_2$, the photosynthetic activity of *Microcystis* depleted the dissolved CO_2 concentration to the nanomolar range and diminished the bicarbonate concentration to ~ 10 μM , while carbonate became the dominant inorganic carbon species (Fig. 4C). This was accompanied by a strong pH increase to ~ 11 (Fig. 4E). Conversely, in the experiments at high $p\text{CO}_2$, dissolved CO_2 was maintained at ~ 10 μM , bicarbonate increased to ~ 3000 μM , and pH remained < 9 (Fig. 4, D and F).

Implementing the CO_2 and bicarbonate concentrations observed at steady state (Fig. 4) into the measured carbon uptake kinetics (Fig. 2) shows that, since the dissolved CO_2 concentration was

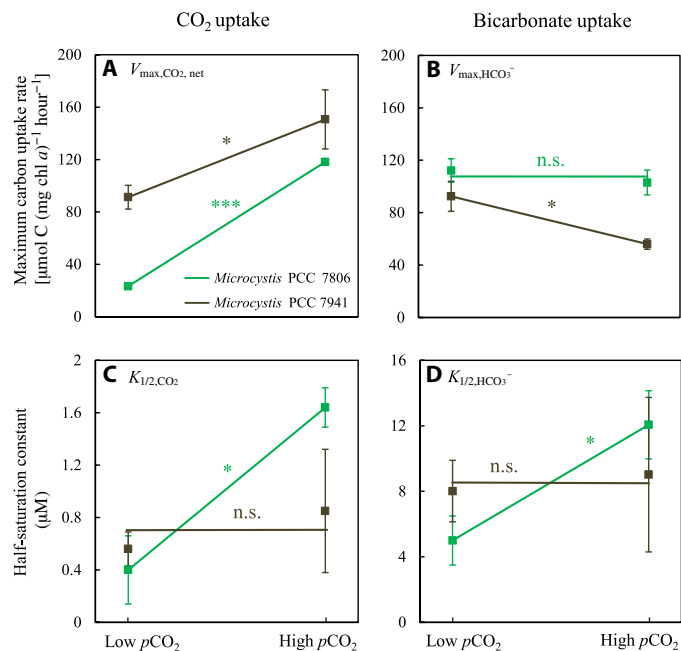


Fig. 3. Reaction norms of the carbon uptake kinetics of *Microcystis* PCC 7806 and PCC 7941. The reaction norms show the plasticity of maximum uptake rates of (A) CO₂ ($V_{\max,CO_2,net}$) and (B) bicarbonate (V_{\max,HCO_3^-}) and the plasticity of half-saturation constants for (C) CO₂ ($K_{1/2,CO_2}$) and (D) bicarbonate ($K_{1/2,HCO_3^-}$), in response to acclimation to either low or high pCO_2 . Data points show parameter values \pm SD obtained by Michaelis-Menten fits to replicated measurements of the carbon uptake kinetics (see Fig. 2 and fig. S1; $n = 4$ for low pCO_2 and $n = 3$ to 4 for high pCO_2). Significant differences between parameter values at low pCO_2 and high pCO_2 were assessed using the independent-samples t test corrected for multiple hypothesis testing (*** $P < 0.001$; * $P < 0.05$; n.s., not significant). Statistical details are reported in table S3.

depleted, the net CO₂ uptake rate was negative in the experiments at low pCO_2 . Hence, carbon fixation at low pCO_2 relied exclusively (100%) on bicarbonate uptake. Carbon fixation in the high pCO_2 experiments relied for ~50% on CO₂ uptake and ~50% on bicarbonate uptake.

The model predictions captured the time courses and steady states of population density, pH, and inorganic carbon chemistry in the chemostats quite well, both for the experiments at low and at high pCO_2 (Fig. 4). Similar results were obtained for the other strain, *Microcystis* PCC 7941 (fig. S2). These results provide proof of principle that, at least under controlled laboratory conditions, measurements of the phenotypic plasticity of carbon fixation rates can be used to quantitatively predict the growth of cyanobacteria at different pCO_2 levels.

The model can be used to quantify how the observed phenotypic plasticity affected cyanobacterial growth. For the experiments at low pCO_2 , model simulations predicted a 14.7% higher population density if the carbon uptake kinetics were acclimated to low pCO_2 than if they were acclimated to high pCO_2 (compare green and gray lines in Fig. 4A). Conversely, for the experiments at high pCO_2 , model simulations predicted a 17.3% higher population density if the carbon uptake kinetics were acclimated to high pCO_2 than if they were acclimated to low pCO_2 (Fig. 4B). Hence, phenotypic plasticity of the carbon uptake kinetics enhanced the population densities of *Microcystis*.

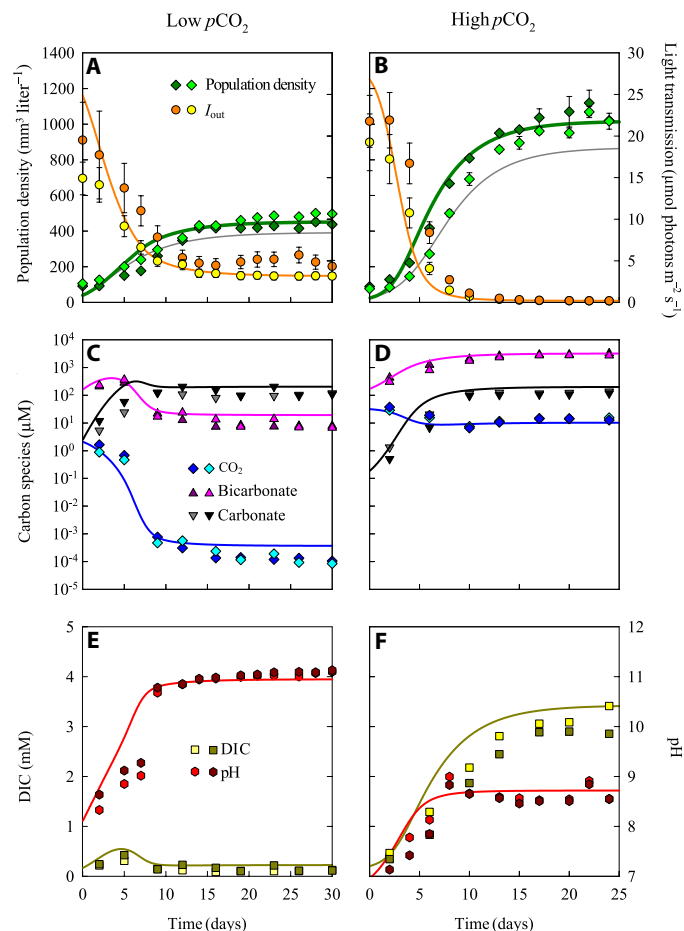


Fig. 4. Population density, inorganic carbon chemistry, and pH in chemostat experiments with *Microcystis* PCC 7806 at low and at high pCO_2 . Chemostat experiments were performed in duplicate, at low pCO_2 (left) and at high pCO_2 (right). (A and B) *Microcystis* population density ($n = 3$ technical replicates per chemostat) and light intensity I_{out} transmitted through the chemostat ($n = 10$). (C and D) Dissolved CO₂, bicarbonate, and carbonate concentrations. (E and F) Dissolved inorganic carbon (DIC) and pH ($n = 3$ technical replicates per chemostat). Symbols indicate experimental data of the duplicate chemostat experiments, error bars indicate SDs of technical replicates, and lines indicate model predictions. Error bars in (E) and (F) did not exceed the size of the symbols. For comparison, gray lines in (A) and (B) are model predictions for nonacclimated cells that either (A) grow at low pCO_2 but with carbon uptake kinetics acclimated to high pCO_2 or (B) grow at high pCO_2 but with carbon uptake kinetics acclimated low pCO_2 . Steady-state characteristics of the experiments are summarized in table S1, and parameter values of the model are listed in tables S4 and S5.

Extrapolation to lakes

To estimate how phenotypic plasticity will affect the response of *Microcystis* blooms in lakes to rising atmospheric pCO_2 , we up-scaled the model from laboratory chemostats to eutrophic lakes. For this purpose, we used the measured carbon uptake kinetics of *Microcystis*, but adjusted system parameters such as mixing depth, light intensity, and dilution rate to a lake context (section S3 and table S6). We compared model predictions for one plastic and two fixed phenotypes of *Microcystis*. The “plastic phenotype” displayed the phenotypic plasticity of *Microcystis* PCC 7806, the “low pCO_2 phenotype” maintained the uptake kinetics measured in the low pCO_2 chemostat, and the “high pCO_2 phenotype” maintained the uptake kinetics measured at high pCO_2 .

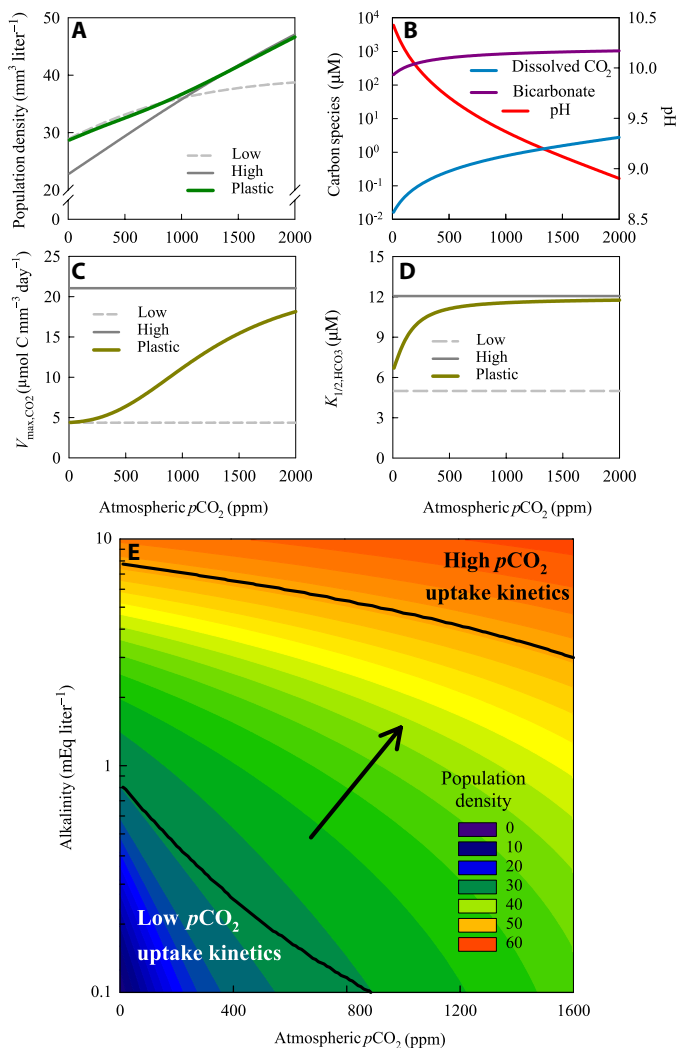


Fig. 5. *Microcystis* blooms predicted for lakes with different atmospheric $p\text{CO}_2$ and alkalinity. (A to D) Model predictions of (A) cyanobacterial population density, (B) dissolved CO_2 concentration, bicarbonate, and pH, (C) maximum net CO_2 uptake rate, and (D) half-saturation constant for bicarbonate uptake in *Microcystis* blooms of eutrophic lakes at different atmospheric $p\text{CO}_2$ and an alkalinity of 1 mEq liter^{-1} . Predictions were made for three phenotypes: a plastic phenotype (green line), a low $p\text{CO}_2$ phenotype (dashed gray line), and a high $p\text{CO}_2$ phenotype (solid gray line). (B) Predictions only for the plastic phenotype. (E) Contour plot of the population density of the plastic phenotype, predicted for eutrophic lakes with different atmospheric $p\text{CO}_2$ and alkalinity. Black lines indicate the parameter regions at which the carbon uptake kinetics of the plastic phenotype have almost fully adjusted ($\geq 90\%$) to either low $p\text{CO}_2$ or high $p\text{CO}_2$. The arrow indicates the transition zone where the plastic phenotype shifts from low $p\text{CO}_2$ to high $p\text{CO}_2$ uptake kinetics. All graphs show model predictions for cyanobacterial blooms at steady state. Species and lake parameters are provided in tables S5 and S6.

The model predicts that rising atmospheric $p\text{CO}_2$ will increase cyanobacterial population densities, dissolved CO_2 , and bicarbonate concentrations and will diminish the development of a very high pH during *Microcystis* blooms (Fig. 5, A and B). Furthermore, the model shows that the plastic phenotype will adjust its carbon uptake kinetics to the prevailing atmospheric $p\text{CO}_2$ and to lake alkalinity (Fig. 5, C to E). More specifically, the plastic phenotype will display carbon uptake kinetics resembling the low $p\text{CO}_2$ phenotype in low-alkaline lakes

and at low atmospheric $p\text{CO}_2$, whereas it will display carbon uptake kinetics resembling the high $p\text{CO}_2$ phenotype in high-alkaline lakes and at high atmospheric $p\text{CO}_2$. In this way, the plastic phenotype is able to maximize its bloom size across the entire $p\text{CO}_2$ gradient, with population densities matching those of the low $p\text{CO}_2$ phenotype at low $p\text{CO}_2$ and those of the high $p\text{CO}_2$ phenotype at high $p\text{CO}_2$ (Fig. 5A). As a consequence, rising atmospheric $p\text{CO}_2$ is predicted to intensify *Microcystis* blooms across a wide range of lakes (Fig. 5E).

DISCUSSION

Our results show a 1.8- to 5-fold increase of the maximum CO_2 uptake rate of *Microcystis* at elevated $p\text{CO}_2$, which greatly exceeds plasticity of the CO_2 uptake rates reported for other freshwater cyanobacteria and green algae (Table 1) and a wide variety of marine phytoplankton species (31). This high flexibility in CO_2 uptake rates is most likely an adaptation to the major changes in CO_2 availability that can be encountered during dense cyanobacterial blooms. Dissolved CO_2 concentrations can change from air-equilibrated or even CO_2 -supersaturated concentrations at the onset of phytoplankton blooms to complete depletion of the available CO_2 in fully developed phytoplankton blooms (11, 14, 32). CO_2 depletion is accompanied by an increase in pH, which shifts the inorganic carbon chemistry toward bicarbonate. Sustained high carbon fixation rates by very dense cyanobacterial blooms may even decrease the bicarbonate concentration and increase pH to >10 (14, 20), shifting the balance from bicarbonate to carbonate as the dominant inorganic carbon species (as in Fig. 4C).

In our chemostat experiments, physiological acclimation occurred within a few weeks, on a similar time scale as the changes in inorganic carbon chemistry induced by the growing cyanobacterial populations. These results imply that the carbon uptake kinetics of cyanobacteria may change drastically during bloom development, from cells with high maximum CO_2 uptake rates but low bicarbonate uptake efficiency when dissolved CO_2 concentrations are still high at the onset of a cyanobacterial bloom, to cells with low maximum CO_2 uptake rates but high bicarbonate uptake efficiency at the peak of the bloom when dissolved CO_2 concentrations have been depleted.

The high maximum CO_2 uptake rate at elevated $p\text{CO}_2$ is offset by down-regulation of the bicarbonate uptake efficiency. Previous results (33) have shown that the high-affinity bicarbonate uptake system BCT1 of *Microcystis* strains is strongly down-regulated at elevated $p\text{CO}_2$, which is a sensible response in view of the energetic costs of this adenosine triphosphate (ATP)-dependent uptake system and likely explains the low bicarbonate uptake efficiency at elevated $p\text{CO}_2$ in our experiments. The maximum bicarbonate uptake rates of the two *Microcystis* strains in our study responded differently to elevated $p\text{CO}_2$, which may be related to the different composition of their bicarbonate uptake systems. Cyanobacteria in which maximum bicarbonate uptake rates were reduced at elevated $p\text{CO}_2$ [*Microcystis* PCC 7941 (19), *Synechocystis* PCC 6803 (22), and *Synechococcus* PCC 7942 (23, 24)] all contain the low-flux bicarbonate transporter SbtA, whereas cyanobacteria in which maximum bicarbonate uptake rates did not respond to changes in $p\text{CO}_2$ [*Microcystis* PCC 7806 (19) and *Trichodesmium erythraeum* IMS101 (25)] all contain the high-flux bicarbonate transporter BicA but lack SbtA. Since carbon uptake kinetics have thus far been investigated for only a few cyanobacteria, these associations should be interpreted with some caution. However, down-regulation of the bicarbonate uptake efficiency by a higher

Table 1. Comparison of the carbon uptake kinetics of freshwater cyanobacteria and green algae measured by MIMS using the chemical disequilibrium assay (29, 30). Units for $K_{1/2}$ and V_{max} are μM and $\mu\text{mol C (mg chl a)}^{-1} \text{hour}^{-1}$, respectively.

Species	Net CO ₂ uptake				Bicarbonate uptake				References
	$K_{1/2, \text{CO}_2}$		$V_{\text{max}, \text{CO}_2, \text{net}}$		$K_{1/2, \text{HCO}_3}$		$V_{\text{max}, \text{HCO}_3}$		
	Low $p\text{CO}_2$	High $p\text{CO}_2$	Low $p\text{CO}_2$	High $p\text{CO}_2$	Low $p\text{CO}_2$	High $p\text{CO}_2$	Low $p\text{CO}_2$	High $p\text{CO}_2$	
Cyanobacteria									
<i>Microcystis aeruginosa</i> PCC 7806	0.4	1.6	23	118	5	12	112	103	This study
<i>Microcystis aeruginosa</i> PCC 7941	0.6	0.9	73	134	8	9	92	55	This study
<i>Synechococcus</i> PCC 7942	0.4	5.6	165	110	15	270	224	126	23
<i>Synechococcus</i> PCC 7942	0.5	3.6	103	116	9	248	230	206	24
<i>Synechocystis</i> PCC 6803	1	3.5	145	173	4.8	86	281	218	22
Green algae									
<i>Chlamydomonas noctigama</i>	3.1	8.1	37	39	75	379	41	37	49
<i>Chlamydomonas reinhardtii</i>	2	15	46	36	26	104	38	60	50
<i>Chlamydomonas reinhardtii</i>	0.9	8.3	113	82	78	316	92	75	51
<i>Scenedesmus obliquus</i>	0.3	4.5	107	105	13	55	34	35	50
<i>Tetraedron minimum</i>	2.1	9.4	11	7	279	841	60	53	49

half-saturation constant and/or lower maximum bicarbonate uptake rate has also been reported for green algae (Table 1) and diatoms (34, 35) and, hence, seems a common response to elevated $p\text{CO}_2$.

Phenotypic plasticity complicates assessments of how natural communities will respond to climate change (1–4), because species responses obtained for one set of environmental conditions may deviate from those obtained for other conditions. Our study illustrates that phenotypic plasticity can be built successfully into models. The model predicts an increase in the maximum CO₂ uptake rate and decrease in the bicarbonate uptake efficiency at elevated $p\text{CO}_2$, in agreement with our experimental results (Figs. 4 and 5). Furthermore, the model reveals the adaptive significance of this phenotypic plasticity, as physiological acclimation to the prevailing $p\text{CO}_2$ conditions enhanced the size of the *Microcystis* population [compare the gray and green lines in Figs. 4 (A and B) and 5A]. Enhanced growth obtained through physiological acclimation may provide a competitive advantage, which likely explains why, in recent competition experiments, *Microcystis* became a strong competitor in comparison to green algae at elevated $p\text{CO}_2$ (36). In total, these results provide strong evidence that the high phenotypic plasticity of the carbon uptake kinetics of *Microcystis* will stimulate the development of *Microcystis* blooms at elevated $p\text{CO}_2$.

In addition to phenotypic plasticity, evolutionary changes are also likely to affect the carbon uptake kinetics of future cyanobacterial blooms. Shifts in genotype composition have been found in selection experiments with multiple strains of *Microcystis* (12). Furthermore,

evolutionary changes in CO₂ uptake rates and growth kinetics have been observed in long-term phytoplankton studies exposed to elevated CO₂ for hundreds to thousands of generations (37, 38). The short time span of our single-strain experiments did not provide much time for de novo mutations and subsequent selection, however. Therefore, the observed changes in our study presumably did not involve evolutionary changes in the carbon uptake kinetics but indeed derived from a high phenotypic plasticity of these traits.

While our study focused on the carbon uptake kinetics of one of the most notorious bloom-forming cyanobacteria, other relevant processes known to affect cyanobacterial blooms were left out of the equations. For example, in addition to rising atmospheric $p\text{CO}_2$, cyanobacterial blooms will also be affected by global warming (5, 6, 13). Higher temperatures will enhance the growth rate of *Microcystis* but reduce the solubility of CO₂, both in nonlinear ways. How this will play out is difficult to predict without dedicated models. Other important processes affecting bloom development include nutrient limitation, lake stratification, and interactions with viruses and other organisms in the aquatic food web (8). Hence, our model does not attempt to describe the full complexity of the natural world. However, our model and its experimental validation do provide an important first step for the implementation of phenotypic plasticity in ecosystem models that do take these other processes into account.

In conclusion, our results demonstrate that incorporation of the phenotypic plasticity of traits improves predictions of species responses to climate change. More specifically, we found that the high

phenotypic plasticity of its CO₂ uptake rate provides the bloom-forming cyanobacterium *Microcystis* with an exceptionally strong capacity to respond to rising pCO₂ levels in comparison to other phytoplankton species. *Microcystis* blooms already cause major water quality problems in Lake Erie (USA) (39), Lake Taihu (China) (40), Lake Victoria (Africa) (41), and many other eutrophic and hypertrophic lakes worldwide. Our findings warn that rising atmospheric pCO₂ will further intensify surface blooms of *Microcystis* in the coming decades.

MATERIALS AND METHODS

Species and culture conditions

We studied the toxic (microcystin-producing) cyanobacteria *Microcystis aeruginosa* PCC 7806 and PCC 7941. Both *Microcystis* strains contain the two known CO₂ uptake systems (NDH-1₃ and NDH-1₄). In addition, *Microcystis* PCC 7941 contains all three known bicarbonate uptake systems (BCT1, SbtA, and BicA), whereas *Microcystis* PCC 7806 has only two of them (BCT1 and BicA) (19).

The *Microcystis* strains were cultured as unialgal but nonaxenic strains, in CO₂-controlled chemostats specifically designed to study the population dynamics of phytoplankton species (11, 12, 42) (Fig. 1A). The chemostats allowed full control of light intensity, temperature, nutrient input, and pCO₂ of the aeration gas. Each chemostat consisted of a flat culture vessel with an optimal path length (mixing depth) of $z_{\max} = 5$ cm and a working volume of ~1.7 liters. The vessel was illuminated from one side to create a unidirectional light gradient, using a constant incident light intensity of 40 μmol photons m⁻² s⁻¹ provided by white fluorescent tubes (Philips PL-L 24W/840/4P, Philips Lighting, Eindhoven, The Netherlands). The temperature was maintained at 25 ± 1°C with a stainless steel cooling finger inside each chemostat and connected to a Colora thermocryostat. To avoid nutrient limitation, we provided a nutrient-rich mineral medium [modified BG-11 medium, (43)], with 8 mM NaNO₃ and 175 μM K₂HPO₄·3H₂O but without addition of Na₂CO₃ or NaHCO₃, at a dilution rate of 0.2 day⁻¹.

The chemostats were aerated with pressurized air containing either 100 ppm pCO₂ ("low pCO₂") or 1000 ppm pCO₂ ("high pCO₂") at a gas flow rate of 30 liters hour⁻¹. At these settings, *Microcystis* growth is mainly limited by inorganic carbon at low pCO₂ and by light at high pCO₂ (table S1; see also 11, 36). The pCO₂ in the gas flow was checked regularly using an Environmental Gas Monitor (EGM-4; PP Systems, Amesbury, MA, USA). The chemostats were sampled every 2 to 3 days to measure population densities, inorganic carbon, nutrients, and light. The chemostats were considered to be in steady state when the coefficient of variation of the population density was less than 10% for at least four consecutive time points.

Carbon uptake kinetics

Carbon uptake kinetics of the two *Microcystis* strains were determined with a MIMS (HPR40, Hiden Analytical Ltd., UK) using the chemical disequilibrium assay (29, 30) after they had grown in the chemostats at either low or high pCO₂ for ~40 days. At this time point, the chemostats were in steady state for ~20 days. Before each assay, fresh *Microcystis* cells were sampled from the steady-state chemostats and concentrated by gentle centrifugation for 5 min at 600g. Then, the supernatant was discarded and the pelleted *Microcystis* cells were resuspended in mineral medium without dissolved inorganic carbon (DIC) and nitrate. The medium was adjusted to pH 8.0 ± 0.1 using 50 mM Hepes buffer. To ensure similar assay conditions, the resuspended *Microcystis* cells

were diluted to an OD₇₅₀ (optical density at 750 nm) of 0.3, which corresponds to a *Microcystis* biovolume of ~400 mm³ liter⁻¹. The suspension was aerated with N₂ gas for at least 1 hour at a temperature of 25°C to remove any residual CO₂. Subsequently, we transferred the *Microcystis* suspension to a 10-ml MIMS cuvette. We added a final concentration of 50 μM membrane-impermeable dextran-bound sulfonamide (Synthelec AB, Lund, Sweden) to inhibit any possible extracellular carbonic anhydrase activity. The MIMS cuvette was provided with the same light intensity (40 μmol photons m⁻² s⁻¹) using the same white fluorescent tubes and was kept at the same temperature (25°C) as the chemostat experiments.

With the MIMS, we simultaneously measured O₂ and CO₂ fluxes during consecutive light-dark intervals (5 min each) after adding known CO₂ and bicarbonate concentrations during each dark phase. Net C fixation rates and respiration rates (r) were measured as rates of O₂ production in the light and O₂ consumption in the dark, respectively, assuming a photosynthetic quotient of 1.0 (i.e., O₂ production equals net C fixation). Net CO₂ uptake rates ($V_{\text{CO}_2,\text{net}}$) were calculated from CO₂ consumption in the light period, corrected for CO₂/bicarbonate interconversion in the medium. Bicarbonate uptake rates (V_{HCO_3}) were calculated from the difference between net C fixation and net CO₂ uptake rates.

The measured CO₂ and bicarbonate uptake rates were fitted to Michaelis-Menten equations

$$V_{\text{CO}_2,\text{net}} = \frac{V_{\text{max,CO}_2,\text{gross}} [\text{CO}_2]}{K_{1/2,\text{CO}_2} + [\text{CO}_2]} - r \quad (3)$$

$$V_{\text{HCO}_3} = \frac{V_{\text{max,HCO}_3} [\text{HCO}_3^-]}{K_{1/2,\text{HCO}_3} + [\text{HCO}_3^-]} \quad (4)$$

where [CO₂] and [HCO₃⁻] are the dissolved CO₂ and bicarbonate concentration, $V_{\text{max,CO}_2,\text{gross}}$ and $V_{\text{max,HCO}_3}$ are the maximum uptake rates of gross CO₂ and bicarbonate, and $K_{1/2,\text{CO}_2}$ and $K_{1/2,\text{HCO}_3}$ are the half-saturation constants. The maximum net CO₂ uptake rate was calculated as $V_{\text{max,CO}_2,\text{net}} = V_{\text{max,CO}_2,\text{gross}} - r$. For *Microcystis* PCC 7941, we extended Eq. 4 with an inhibition term to capture the asymptotic decrease of its bicarbonate uptake rate at high bicarbonate concentrations (section S1 and fig. S1, C and D).

Differences between Michaelis-Menten parameters at low pCO₂ versus high pCO₂ were tested for significance using the independent samples t test, corrected for unequal variances when necessary and for multiple hypothesis testing using the false discovery rate (44).

Sampling and analysis

In each sample, the population density of *Microcystis* (expressed by the biovolume of the population) was measured in triplicate with a CASY TTC automated cell counter with a 60-μm capillary (OLS OMNI Life Science, Bremen, Germany). Light intensity transmitted through the chemostat (I_{out}) was measured at the back surface of the chemostat vessel with a LI-COR LI-250 quantum photometer (LI-COR Biosciences, Lincoln, NE, USA). pH was measured with a SCHOTT pH meter (SCHOTT AG, Mainz, Germany) immediately after sampling. DIC was measured as CO₂ after addition of 25% phosphoric acid using a Model 700 TOC Analyzer (OI Corp., College Station, TX, USA). From DIC and pH, we calculated CO₂(aq), bicarbonate, and carbonate concentrations, based on the dissociation constants of inorganic carbon corrected for temperature and salinity (45). Nutrient uptake by cyanobacteria affects alkalinity (11, 46). Our model therefore

required measurement of cellular nutrients, which were determined by gently washing filtered *Microcystis* cells twice with a nutrient-free 15 mM NaCl solution. The washed filters were stored at -20°C until further analysis. For cellular C, N, and S contents, one set of pre-weighted filters were freeze dried, wrapped in tin foil discs (30 mm, Sercon Ltd., Crewe, UK), and analyzed using a Vario EL Elemental Analyzer (Elementar Analysensysteme GmbH, Hanau, Germany). For the cellular P content, another set of the same filters were put into glass tubes that contained 10 ml of Milli-Q water, 0.2 ml of 5.5 M H_2SO_4 , and 1.5 ml of 8% $(\text{NH}_4)_2\text{S}_2\text{O}_8$ solvent, and the sealed tubes were autoclaved for 1 hour at 121°C , to convert all organic P to orthophosphate. Orthophosphate concentrations were measured with a Skalar SA 400 autoanalyzer (Skalar Analytical B.V., Breda, The Netherlands). Samples for chlorophyll *a* analysis were filtered on 25-mm glass fiber filters (GF/C, 1.2- μm pore size, Whatman GmbH, Dassel, Germany) and freeze dried for at least 2 hours. Chlorophyll *a* was extracted with *N,N*-dimethylformamide and measured spectrophotometrically (47).

Mathematical model

We developed a dynamical model to describe the carbon uptake kinetics and population dynamics of cyanobacteria as a function of $p\text{CO}_2$ and light availability. The model combines previous theoretical and experimental work on phytoplankton growth under light-limited (42, 48) and carbon-limited conditions (11, 36). In short, the model assumes eutrophic conditions, in which all nutrients are in ample supply and, hence, do not limit phytoplankton growth. The CO_2 and bicarbonate uptake kinetics and phenotypic plasticity of the uptake parameters are described by Eqs. 1 to 4. The carbon uptake rates and light availability, in turn, determine the growth rate of the cyanobacterial population. Furthermore, uptake of CO_2 , bicarbonate, and nutrients induces changes in pH and alkalinity. These changes in pH and alkalinity affect the speciation of inorganic carbon, which, in turn, feeds back on carbon uptake and growth of the cyanobacteria. The expanding cyanobacterial population also increases the turbidity of the water column, thereby diminishing light available for further photosynthesis and growth. The model is described in full detail in section S2.

The model parameters were measured experimentally and include system parameters (e.g., incident light intensity, $p\text{CO}_2$ level in the gas flow, and dilution rate of the chemostats; table S4) and species parameters (e.g., maximum uptake rates and half-saturation constants; table S5). In particular, the carbon uptake kinetics and respiration rates measured by MIMS (Fig. 2 and tables S2 and S3) served as input to predict the carbon uptake and concomitant changes in inorganic carbon chemistry at both low and high $p\text{CO}_2$. The model and its parameterization are described in detail in section S2.

For the lake model (section S3), we choose parameter values representative for the summer situation in eutrophic lakes dominated by dense *Microcystis* blooms. The species parameters are identical to those of *Microcystis* PCC 7806 (table S5), where we distinguished between a plastic phenotype, low $p\text{CO}_2$ phenotype, and high $p\text{CO}_2$ phenotype as described in Results. The system parameters for the lake model are summarized in table S6.

SUPPLEMENTARY MATERIALS

Supplementary material for this article is available at <http://advances.sciencemag.org/cgi/content/full/6/8/eaax2926/DC1>

Section S1. Description of bicarbonate uptake of *Microcystis* PCC 7941

Section S2. Description of the mathematical model

Section S3. Extrapolation of the model to lakes

Fig. S1. Carbon uptake kinetics of *Microcystis* PCC 7941 acclimated to either low or high $p\text{CO}_2$.
Fig. S2. Population density, inorganic carbon chemistry, and pH in chemostat experiments with *Microcystis* PCC 7941 at low and at high $p\text{CO}_2$.

Table S1. Steady-state characteristics of the chemostat experiments with *Microcystis* PCC 7806 and *Microcystis* PCC 7941.

Table S2. Kinetic parameters estimated from the carbon uptake experiments with *Microcystis* PCC 7806 and *Microcystis* PCC 7941.

Table S3. Tests of significant differences between kinetic parameters estimated at low versus high $p\text{CO}_2$.

Table S4. System parameters applied in the chemostat experiments.

Table S5. Species parameters measured experimentally.

Table S6. System parameters applied in the lake model.

References (52–59)

REFERENCES AND NOTES

1. A. Charmantier, R. H. McCleery, L. R. Cole, C. Perrins, L. E. Kruuk, B. C. Sheldon, Adaptive phenotypic plasticity in response to climate change in a wild bird population. *Science* **320**, 800–803 (2008).
2. L.-M. Chevin, S. Collins, F. Lefèvre, Phenotypic plasticity and evolutionary demographic responses to climate change: taking theory out to the field. *Funct. Ecol.* **27**, 967–979 (2013).
3. C. A. Vargas, N. A. Lagos, M. A. Lardies, C. Duarte, P. H. Manriquez, V. M. Aguilera, B. Broitman, S. Widdicombe, S. Dupont, Species-specific responses to ocean acidification should account for local adaptation and adaptive plasticity. *Nat. Ecol. Evol.* **1**, 0084 (2017).
4. C. T. Kremer, S. B. Fey, A. A. Arellano, D. A. Vasseur, Gradual plasticity alters population dynamics in variable environments: Thermal acclimation in the green alga *Chlamydomonas reinhardtii*. *Proc. Biol. Sci.* **285**, 20171942 (2018).
5. H. W. Paerl, J. Huisman, Blooms like it hot. *Science* **320**, 57–58 (2008).
6. J. M. O’Neil, T. W. Davis, M. A. Burford, C. J. Gobler, The rise of harmful cyanobacteria blooms: potential role of eutrophication and climate change. *Harmful Algae* **14**, 313–334 (2012).
7. Z. E. Taranu, I. Gregory-Eaves, P. R. Leavitt, L. Bunting, T. Buchaca, J. Catalan, I. Domaizon, P. Guilizzoni, A. Lami, S. McGowan, H. Moorhouse, G. Morabito, F. R. Pick, M. A. Stevenson, P. L. Thompson, R. D. Vinebrooke, 2015. Acceleration of cyanobacterial dominance in north temperate-subarctic lakes during the Anthropocene. *Ecol. Lett.* **18**, 375–384 (2015).
8. J. Huisman, G. A. Codd, H. W. Paerl, B. W. Ibelings, J. M. H. Verspagen, P. M. Visser, Cyanobacterial blooms. *Nat. Rev. Microbiol.* **16**, 471–483 (2018).
9. W. W. Carmichael, Health effects of toxin-producing cyanobacteria: “The CyanoHABs”. *Hum. Ecol. Risk Assess.* **7**, 1393–1407 (2001).
10. J. Meriluoto, L. Spoof, G. A. Codd, *Handbook of Cyanobacterial Monitoring and Cyanotoxin Analysis* (John Wiley & Sons Inc., 2017).
11. J. M. H. Verspagen, D. B. Van de Waal, J. F. Finke, P. M. Visser, E. van Donk, J. Huisman, Rising CO_2 levels will intensify phytoplankton blooms in eutrophic and hypertrophic lakes. *PLOS ONE* **9**, e104325 (2014).
12. G. Sandrini, X. Ji, J. M. H. Verspagen, R. P. Tann, P. C. Slot, V. M. Luimstra, J. M. Schuurmans, H. C. P. Matthijs, J. Huisman, Rapid adaptation of harmful cyanobacteria to rising CO_2 . *Proc. Natl. Acad. Sci. U.S.A.* **113**, 9315–9320 (2016).
13. P. M. Visser, J. M. H. Verspagen, G. Sandrini, L. J. Stal, H. C. P. Matthijs, T. W. Davis, H. W. Paerl, J. Huisman, How rising CO_2 and global warming may stimulate harmful cyanobacterial blooms. *Harmful Algae* **54**, 145–159 (2016).
14. B. W. Ibelings, S. C. Maberly, Photoinhibition and the availability of inorganic carbon restrict photosynthesis by surface blooms of cyanobacteria. *Limnol. Oceanogr.* **43**, 408–419 (1998).
15. R. Wanninkhof, M. Knox, Chemical enhancement of CO_2 exchange in natural waters. *Limnol. Oceanogr.* **41**, 689–697 (1996).
16. M. R. Badger, G. D. Price, CO_2 concentrating mechanisms in cyanobacteria: Molecular components, their diversity and evolution. *J. Exp. Bot.* **54**, 609–622 (2003).
17. R. L. Burnap, M. Hagemann, A. Kaplan, Regulation of CO_2 concentrating mechanism in cyanobacteria. *Life* **5**, 348–371 (2015).
18. G. D. Price, M. R. Badger, F. J. Woodger, B. M. Long, Advances in understanding the cyanobacterial CO_2 -concentrating-mechanism (CCM): functional components, C_4 transporters, diversity, genetic regulation and prospects for engineering into plants. *J. Exp. Bot.* **59**, 1441–1461 (2008).
19. G. Sandrini, H. C. P. Matthijs, J. M. H. Verspagen, G. Muijzer, J. Huisman, Genetic diversity of inorganic carbon uptake systems causes variation in CO_2 response of the cyanobacterium *Microcystis*. *ISME J.* **8**, 589–600 (2014).
20. G. Sandrini, R. P. Tann, J. M. Schuurmans, S. A. M. van Beusekom, H. C. P. Matthijs, J. Huisman, Diel variation in gene expression of the CO_2 -concentrating mechanism during a harmful cyanobacterial bloom. *Front. Microbiol.* **7**, 551 (2016).
21. M. Eisenhut, E. A. von Wobeser, L. Jonas, H. Schubert, B. W. Ibelings, H. Bauwe, H. C. P. Matthijs, M. Hagemann, Long-term response toward inorganic carbon limitation

- in wild type and glycolate turnover mutants of the cyanobacterium *Synechocystis* sp. strain PCC 6803. *Plant Physiol.* **144**, 1946–1959 (2007).
22. J. J. Benschop, M. R. Badger, G. D. Price, Characterisation of CO₂ and HCO₃⁻ uptake in the cyanobacterium *Synechocystis* sp. PCC6803. *Photosynth. Res.* **77**, 117–126 (2003).
 23. J. W. Yu, G. D. Price, M. R. Badger, A mutant isolated from the cyanobacterium *Synechococcus* PCC7942 is unable to adapt to low inorganic carbon conditions. *Plant Physiol.* **104**, 605–611 (1994).
 24. D. Sültemeyer, B. Klughammer, M. R. Badger, G. D. Price, Fast induction of high-affinity HCO₃⁻ transport in cyanobacteria. *Plant Physiol.* **116**, 183–192 (1998).
 25. S. A. Kranz, D. Sültemeyer, K. U. Richter, B. Rost, Carbon acquisition by *Trichodesmium*: The effect of pCO₂ and diurnal changes. *Limnol. Oceanogr.* **54**, 548–559 (2009).
 26. B. M. Hopkinson, J. N. Young, A. L. Tansik, B. J. Binder, The minimal CO₂ concentrating mechanism of *Prochlorococcus* spp. MED4 is effective and efficient. *Plant Physiol.* **166**, 2205–2217 (2014).
 27. M. J. Harke, M. M. Steffen, C. J. Gobler, T. G. Otten, S. W. Wilhelm, S. A. Wood, H. W. Paerl, A review of the global ecology, genomics, and biogeography of the toxic cyanobacterium, *Microcystis* spp. *Harmful Algae* **54**, 4–20 (2016).
 28. S. Sobek, L. J. Tranvik, J. J. Cole, Temperature independence of carbon dioxide supersaturation in global lakes. *Glob. Biogeochem. Cycles* **19**, GB2003 (2005).
 29. M. R. Badger, K. Palmqvist, J.-W. Yu, Measurement of CO₂ and HCO₃⁻ fluxes in cyanobacteria and microalgae during steady-state photosynthesis. *Physiol. Plant.* **90**, 529–536 (1994).
 30. B. Rost, S. A. Kranz, K. U. Richter, P. D. Tortell, Isotope disequilibrium and mass spectrometric studies of inorganic carbon acquisition by phytoplankton. *Limnol. Oceanogr. Methods* **5**, 328–337 (2007).
 31. D. B. van de Waal, K. M. Brandenburg, J. Keuskamp, S. Trimborn, S. Rokitta, S. A. Kranz, B. Rost, Highest plasticity of carbon concentrating mechanisms in earliest evolved phytoplankton. *Limnol. Oceanogr. Lett.* **4**, 37–43 (2019).
 32. S. C. Maberly, Diel, episodic and seasonal changes in pH and concentrations of inorganic carbon in a productive lake. *Freshw. Biol.* **35**, 579–598 (1996).
 33. G. Sandrini, S. Cunsolo, J. M. Schuurmans, H. C. P. Matthijs, J. Huisman, Changes in gene expression, cell physiology and toxicity of the harmful cyanobacterium *Microcystis aeruginosa* at elevated CO₂. *Front. Microbiol.* **6**, 401 (2015).
 34. B. Rost, U. Riebesell, S. Burkhardt, D. Sültemeyer, Carbon acquisition of bloom-forming marine phytoplankton. *Limnol. Oceanogr.* **48**, 55–67 (2003).
 35. S. Trimborn, D. Wolf-Gladrow, K.-U. Richter, B. Rost, The effect of pCO₂ on carbon acquisition and intracellular assimilation in four marine diatoms. *J. Exp. Mar. Biol. Ecol.* **376**, 26–36 (2009).
 36. X. Ji, J. M. H. Verspagen, M. Stomp, J. Huisman, Competition between cyanobacteria and green algae at low versus elevated CO₂: Who will win, and why? *J. Exp. Bot.* **68**, 3815–3828 (2017).
 37. S. Collins, G. Bell, Phenotypic consequences of 1000 generations of selection at elevated CO₂ in a green alga. *Nature* **431**, 566–569 (2004).
 38. D. A. Hutchins, N. G. Walworth, E. A. Webb, M. A. Saito, D. Moran, M. R. McIlvin, J. Gale, F.-X. Fu, Irreversibly increased nitrogen fixation in *Trichodesmium* experimentally adapted to elevated carbon dioxide. *Nat. Commun.* **6**, 8155 (2015).
 39. G. S. Bullerjahn, R. M. McKay, T. W. Davis, D. B. Baker, G. L. Boyer, L. V. D'Anglada, G. J. Doucette, J. C. Ho, E. G. Irwin, C. L. Kling, R. M. Kudela, R. Kurmayer, A. M. Michalak, J. D. Ortiz, T. G. Otten, H. W. Paerl, B. Qin, B. L. Sohngen, R. P. Stumpf, P. M. Visser, S. W. Wilhelm, Global solutions to regional problems: collecting global expertise to address the problem of harmful cyanobacterial blooms, a Lake Erie case study. *Harmful Algae* **54**, 223–238 (2016).
 40. L. Guo, Doing battle with the green monster of Taihu Lake. *Science* **317**, 1166–1166 (2007).
 41. L. Sitoki, R. Kurmayer, E. Rott, Spatial variation of phytoplankton composition, biovolume, and resulting microcystin concentrations in the Nyanza Gulf (Lake Victoria, Kenya). *Hydrobiologia* **691**, 109–122 (2012).
 42. J. Huisman, R. R. Jonker, C. Zonneveld, F. J. Weissing, Competition for light between phytoplankton species: Experimental tests of mechanistic theory. *Ecology* **80**, 211–222 (1999).
 43. R. Rippka, J. Deruelles, J. B. Waterbury, M. Herdman, R. Y. Stanier, Generic assignments, strain histories and properties of pure cultures of cyanobacteria. *Microbiology* **111**, 1–61 (1979).
 44. Y. Benjamini, D. Yekutieli, The control of the false discovery rate in multiple testing under dependency. *Ann. Stat.* **29**, 1165–1188 (2001).
 45. W. Stumm, J. J. Morgan, *Aquatic Chemistry: Chemical Equilibria and Rates in Natural Waters* (Wiley and Sons, 1996).
 46. D. A. Wolf-Gladrow, R. E. Zeebe, C. Klaas, A. Kortzinger, A. G. Dickson, Total alkalinity: the explicit conservative expression and its application to biogeochemical processes. *Mar. Chem.* **106**, 287–300 (2007).
 47. R. J. Porra, W. A. Thompson, P. E. Kriedemann, Determination of accurate extinction coefficients and simultaneous equations for assaying chlorophylls *a* and *b* extracted with four different solvents: Verification of the concentration of chlorophyll standards by atomic absorption spectroscopy. *Biochim. Biophys. Acta* **975**, 384–394 (1989).
 48. J. Huisman, F. J. Weissing, Light-limited growth and competition for light in well-mixed aquatic environments: an elementary model. *Ecology* **75**, 507–520 (1994).
 49. E. van Hunnik, G. Amoroso, D. Sültemeyer, Uptake of CO₂ and bicarbonate by intact cells and chloroplasts of *Tetradron minimum* and *Chlamydomonas noctigama*. *Planta* **215**, 763–769 (2002).
 50. K. Palmqvist, J.-W. Yu, M. R. Badger, Carbonic anhydrase activity and inorganic carbon fluxes in low- and high-C_i cells of *Chlamydomonas reinhardtii* and *Scenedesmus obliquus*. *Physiol. Plant.* **90**, 537–547 (1994).
 51. G. Amoroso, D. Sültemeyer, C. Thyssen, H. P. Fock, Uptake of HCO₃⁻ and CO₂ in cells and chloroplasts from the microalgae *Chlamydomonas reinhardtii* and *Dunaliella tertiolecta*. *Plant Physiol.* **116**, 193–201 (1998).
 52. U. Siegenthaler, J. L. Sarmiento, Atmospheric carbon dioxide and the ocean. *Nature* **365**, 119–125 (1993).
 53. J. J. Cole, D. L. Bade, D. Bastviken, M. L. Pace, M. van de Bogert, Multiple approaches to estimating air-water gas exchange in small lakes. *Limnol. Oceanogr. Methods* **8**, 285–293 (2010).
 54. R. Portielje, L. Lijklema, Carbon dioxide fluxes across the air-water interface and its impact on carbon availability in aquatic systems. *Limnol. Oceanogr.* **40**, 690–699 (1995).
 55. H. C. Frey, S. R. Patil, Identification and review of sensitivity analysis methods. *Risk Anal.* **22**, 553–578 (2002).
 56. D. L. Bade, J. J. Cole, Impact of chemically enhanced diffusion on dissolved inorganic carbon stable isotopes in a fertilized lake. *J. Geophys. Res.* **111**, C01014 (2006).
 57. K. D. Jöhnk, J. Huisman, J. Sharples, B. Sommeijer, P. M. Visser, J. M. Stroom, Summer heatwaves promote blooms of harmful cyanobacteria. *Glob. Chang. Biol.* **14**, 495–512 (2008).
 58. H. Xu, H. W. Paerl, B. Qin, G. Zhu, G. Gao, Nitrogen and phosphorus inputs control phytoplankton growth in eutrophic Lake Taihu, China. *Limnol. Oceanogr.* **55**, 420–432 (2010).
 59. J. Crusius, R. Wanninkhof, Gas transfer velocities measured at low wind speed over a lake. *Limnol. Oceanogr.* **48**, 1010–1017 (2003).

Acknowledgments: We thank R. van Hall for assistance with the TOC Analyzer and Elemental Analyzer. **Funding:** This research is supported by the Division of Earth and Life Sciences (ALW) of the Netherlands Organization for Scientific Research (NWO). X.J. is also supported by the National Key R&D Program of China (2017YFC0506001) and the National Natural Science Foundation of China (41676084). **Author contributions:** X.J., J.M.H.V., and J.H. designed the study. X.J. performed the laboratory experiments and analyzed the chemostat samples, with J.M.H.V. providing scientific support. X.J., D.B.V.d.W., and B.R. developed the MIMS bioassay. X.J. performed the MIMS measurements, and X.J., J.M.H.V., D.B.V.d.W., and B.R. analyzed the MIMS data. J.M.H.V. and J.H. developed the model, and J.M.H.V. ran the model predictions. X.J., J.M.H.V., and J.H. wrote the manuscript, and all authors commented on the final version. **Competing interests:** The authors declare that they have no competing interests. **Data and materials availability:** All data needed to evaluate the conclusions in the paper are present in the paper and/or the Supplementary Materials. Additional data related to this paper may be requested from the authors.

Submitted 11 March 2019
Accepted 26 November 2019
Published 19 February 2020
10.1126/sciadv.aax2926

Citation: X. Ji, J. M. H. Verspagen, D. B. Van de Waal, B. Rost, J. Huisman, Phenotypic plasticity of carbon fixation stimulates cyanobacterial blooms at elevated CO₂. *Sci. Adv.* **6**, eaax2926 (2020).